



Cite this: DOI: 10.1039/d1nj02140k

Design and synthesis of a new magnetic metal organic framework as a versatile platform for immobilization of acidic catalysts and CO₂ fixation reaction†

 Faezeh Taghavi,^{‡,ab} Amir Khojastehnezhad,^{‡,ab} Reza Khalifeh,^{‡,c} Maryam Rajabzadeh,^c Fahimeh Rezaei,^c Khalil Abnous^{‡,ab} and Seyed Mohammad Taghdisi^{‡,de}

In this study, a new magnetic metal organic framework (MNP@MOF) with a core-shell structure has been introduced as an efficient and versatile platform for immobilization of Preyssler (H₁₄INaP₅W₃₀O₁₁₀) heteropolyacid (PR HPA). The chemical structure of the nanocatalyst was analyzed by using different techniques, including HRTEM, TEM, HRTEM mapping, SEM, EDX, TGA, XRD, VSM, BET and ICP. These analyses confirmed the core-shell and spherical structure of the catalyst and successful immobilization of PR HPA on its surface. After complete characterization, the efficiency of the catalyst was tested for the synthesis of cyclic carbonates by the chemical fixation of carbon dioxide. Different epoxides were converted to cyclic carbonates in the presence of 0.4 mol% of catalyst and a 0.3 MPa CO₂ pressure under solvent-free conditions. To date, this reaction has been performed with various heterogeneous catalysts, but this is the first report on the use of PR HPA and MNP@MOF for this reaction.

 Received 2nd May 2021,
 Accepted 15th July 2021

DOI: 10.1039/d1nj02140k

rsc.li/njc

Introduction

Nowadays, “global warming” has become a serious problem due to the increase of the CO₂ content in the atmosphere.^{1,2} So, the conversion of carbon dioxide into the useful chemistry materials is one of the main goals in environmental chemistry.³ In this regard, the incorporation of carbon dioxide into the epoxide compounds and, consequently, the production of 5-membered cyclic carbonates is the best way to solve the above-mentioned problem.⁴ Carbonate derivatives are found in natural products and possess different worthwhile applications such as building blocks in organic synthesis, electrolytes in batteries, raw materials for cosmetics, green solvents, polymers, and pharmaceuticals.^{5–8} During the past few decades, extensive attempts have been

performed to present new catalytic systems for the chemical fixation of CO₂,^{9–13} although owing to the high importance of this reaction, the development of new methods is highly recommended.

Currently, Fe₃O₄ magnetic nanoparticles (MNPs) have received widespread attention due to their superparamagnetic properties, high chemical stability, high Curie temperature, and low toxicity.^{14,15} On the other hand, due to their magnetic, mechanical and electrical features and also easy separation process, they have great potential for use in different fields of science and technology, especially heterogeneous catalysis.^{16–23} However, because of the high magnetic capacities, serious aggregations are observed in these unique materials, which is one of the most significant limitations.^{24,25} In order to overcome these shortcomings, a coating process of MNPs can be an excellent approach for the synthesis of well-dispersed MNPs with high magnetic properties.^{26–30} On this basis, MNPs are coated with different organic and inorganic materials such as silica, polymers, carbon materials, covalent organic frameworks (COFs) or especially MOFs.^{31–36} These materials are used as shell structures to control the growth and better dispersion of MNPs. More importantly, the design of core-shell magnetic microspheres with nucleophilic or electrophilic functional groups on the shell can lead to the preparation of various acidic or basic catalysts,^{37–41} because these functional groups, such as hydroxyl, amine, carboxyl or halide groups, have the potential to connect to a wide variety of organic and inorganic ligands by physical and chemical interactions.^{42–44}

^a Pharmaceutical Research Center, Pharmaceutical Technology Institute, Mashhad University of Medical Sciences, Mashhad, Iran.

E-mail: akhojastehnezhad@yahoo.com, abnouskh@mums.ac.ir

^b Department of Medicinal Chemistry, School of Pharmacy, Mashhad University of Medical Sciences, Mashhad, Iran

^c Department of Chemistry, Shiraz University of Technology, Shiraz, 71555-313, Iran

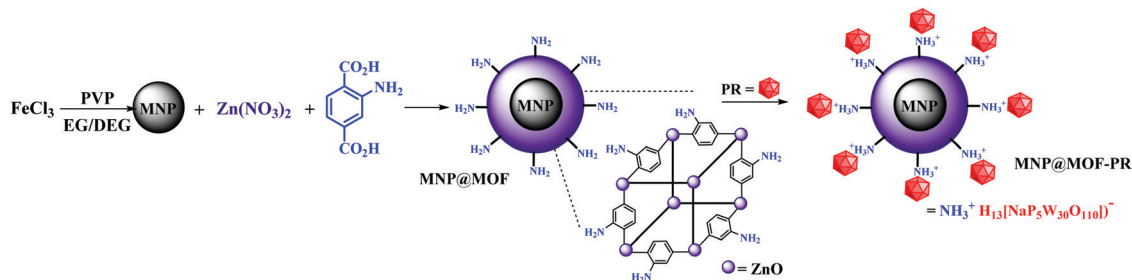
^d Targeted Drug Delivery Research Center, Pharmaceutical Technology Institute, Mashhad University of Medical Sciences, Mashhad, Iran.

E-mail: taghdisihm@mums.ac.ir

^e Department of Pharmaceutical Biotechnology, School of Pharmacy, Mashhad University of Medical Sciences, Mashhad, Iran

† Electronic supplementary information (ESI) available. See DOI: 10.1039/d1nj02140k

‡ These authors contributed equally to this work.



Scheme 1 Preparation of the catalyst (MNP@MOF-PR).

In the traditional heterogeneous catalysts, SiO_2 , Al_2O_3 or TiO_2 , carbon materials and polymer substances have been extensively employed as shell structures and have linked covalently to a number of ligands and been exploited in organic synthesis.^{45–51} Thus, it is of prime importance to offer new magnetic shell platforms with different functional groups to develop the heterogeneous catalysts.

MOFs are reputed as coordination crystalline materials, in which the frameworks are constructed based on polyfunctional organic linkers and inorganic nodes.^{52,53} In recent decades, these porous materials have attracted considerable research attention, not only due to their huge internal surface areas, large density of active sites, high porosity and tailorable properties, but also for wide noteworthy applications in biomedical technology, sensing platforms, energy storage, environmental pollution, and particularly catalysis.^{54–61} For example, Ke *et al.* reported the synthesis of core-shell magnetic MOFs ($\text{Fe}_3\text{O}_4@$ MIL-100(Fe)) as an excellent catalyst for the Claisen-Schmidt condensation reaction.⁶² Chang and co-workers developed the preparation of AgNP-embedded $\text{Fe}_3\text{O}_4@$ MOFs (MIL-100(Fe)) with core-shell structures for the catalytic reduction of 4-nitrophenol.⁶³ In another study, Movahedi and colleagues introduced a magnetic and acidic IRMOF catalyst. They designed a sulfamic acid-functionalized Fe_3O_4 -IRMOF nanocomposite for the synthesis of benzopyranopyrimidine derivatives.⁶⁴

Thereby, in this study, a magnetic MOF with amine functional groups (IRMOF-3) on its shell structure was developed as a new platform for immobilization of PR ($\text{H}_{14}[\text{NaP}_5\text{W}_{30}\text{O}_{110}]$) HPA (Scheme 1). This acidic and novel catalyst can convert different aromatic and aliphatic epoxides to cyclic carbonates in the presence of CO_2 pressure of 0.3 MPa and under solvent-free conditions (Scheme 2). It is worth mentioning that, to the best of our knowledge, there are no published reports for the chemical fixation of carbon dioxide with the use of PR HPA-immobilized magnetic MOFs.



R = a: C_6H_5 ; b: 3,4-di CH_3 - C_6H_5 - OCH_2 ; c: 4-isopropyl- C_6H_5 - OCH_2 d: 4-Br- C_6H_5 - OCH_2
e: C_6H_5 - OCH_2 f: methyl methacrylate g: BrCH_2 h: ClCH_2 i: cyclohexane

Scheme 2 Synthesis of cyclic carbonates in the presence of MNP@MOF-PR.

Results and discussion

Briefly, in this project, a new MNP@MOF with a core-shell structure has been introduced as an efficient and versatile platform for immobilization of PR HPA, an either Brønsted or Lewis acid catalyst (Scheme 1). In a previous report, Tang and co-workers reported these MOF structures (IRMOF-3) for coating palladium NPs.⁶⁵ Afterwards, Zhang *et al.* and also Movahedi and colleagues developed the synthesis of magnetic IRMOF-3 for catalytic applications; however, they were not able to achieve the synthesis of core-shell magnetic MOFs, especially IRMOF-3,^{64,66} and they only synthesized magnetic MOFs with composite structures. Thus, in this research, at first, Fe_3O_4 MNPs were synthesized by using FeCl_3 and a hydrothermal process,⁶⁷ and then, these synthesized MNPs with a size below 50 nm were coated with amino-functionalized MOFs (IRMOF-3) by the solvothermal reaction of zinc nitrate and 2-aminoterephthalic acid.⁶⁵ Eventually, PR HPA was immobilized into the amine groups on the surface of the core-shell MNP@MOFs by ionic bonds and the final catalyst (MNP@MOF-PR) was prepared (Scheme 1).^{68–70} The structure of the catalyst was characterized by using different techniques, including HRTEM, TEM, HRTEM mapping, SEM, EDX, TGA, XRD, VSM, BET, and ICP, and explained in the following sections.

First, all the steps for the preparation of magnetic core-shell catalysts were analyzed by FT-IR spectroscopy (Fig. 1 and Fig. S1–S5, ESI[†]). In the first spectrum related to Fe_3O_4 MNPs (Fig. 1a), there are two distinct sharp peaks at 3414 and 569 cm^{-1} that are attributed to the O–H stretching bands of the hydroxyl functional groups on the surface of MNPs and Fe–O bonds into the structure of MNPs, respectively.⁶⁷ In the next spectrum corresponding to MOFs (Fig. 1b), the existence of two characteristic peaks at 3448 and 3337 cm^{-1} is assigned to the asymmetric and symmetric stretching vibrations of amine groups and the strong peaks at 1577 and 1257 cm^{-1} are ascribed to the stretching vibrations of –COOH and C–N groups, respectively.^{64,66} Interestingly, the third spectrum related to MNP@MOF exhibited all characteristic peaks of MOF structures and due to the interactions between MNPs and MOFs, all peaks are shifted to lower wavenumber (blue shift) (for example, 3448–3431 and 3337–3322 in the amine moieties). These observations show that the amino functional groups in the MOF structures are completely retained. So, the use of the simple mixed solvothermal method is a great route to build the well-defined core-shell MNP@MOF structures. Afterwards, the fourth spectrum of PR HPA (Fig. 1d) exhibited

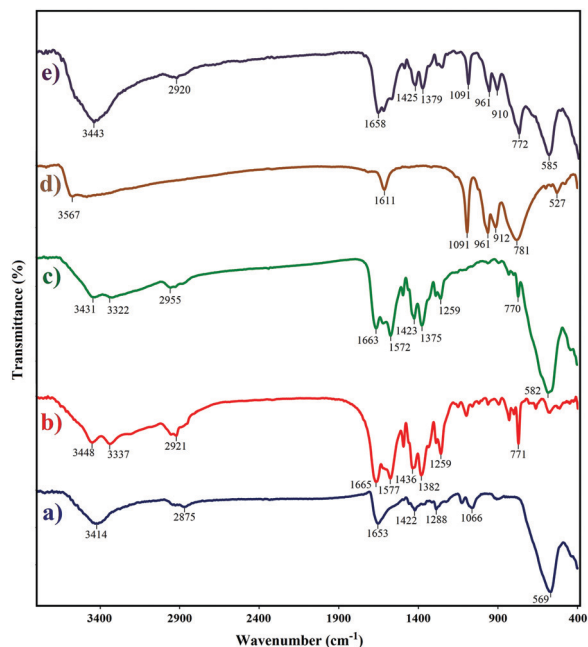


Fig. 1 FT-IR spectra of (a) Fe_3O_4 MNPs, (b) MOF, (c) MNP@MOF, (d) PR HPA and (e) MNP@MOF-PR.

distinct vibrations at 527 and 1091 cm^{-1} for P-O bending and stretching, respectively, 961 and 912 cm^{-1} for W-O-W stretching and 781 cm^{-1} for W=O stretching in the PR structures.⁷⁰ Finally, in the final spectrum of PR HPA immobilized on MNP@MOF (MNP@MOF-PR, Fig. 1e), there are all the characteristic peaks of PR and MOFs and it is worth mentioning that the two peaks related to the amine groups in the third spectrum are converted

to one sharp peak that confirmed the successful ionic bonding of PR HPA on the amine groups of the MOF structures.^{71,72}

HRTEM, TEM, HRTEM mapping, SEM and also EDX analyses were used to evaluate the morphology and size and investigate the core-shell structures and PR HPA immobilization (Fig. 2–4). As shown in Fig. 1, all the electron microscopic analyses confirmed the spherical and core-shell structures for the magnetic MOF catalyst (Fig. 2). As it is evident from the SEM images (Fig. 1a and b), the morphology of the nanomagnetic structures was somewhat changed after the coating process, and also, the TEM and HRTEM images (Fig. 2c–e) confirmed the successful formation of core-shell structures and proper linkage of PR HPA on the surface of the MNP@MOF structures (darker points in Fig. 2e).^{73,74} These observations were similar to the previous study about the immobilization of heteropolytungstate on amino-functionalized core-shell MNPs.⁷⁵ Besides, for further confirmation of the core-shell nanostructures, selected area electron diffraction (SAED) analysis was performed and is shown in Fig. 2f.⁷⁶

Another great analysis to confirm the core-shell structures and elemental analysis is HRTEM mapping (Fig. 3). This figure obviously showed the core-shell structures of magnetic MOFs with all elements including iron and oxygen for the core moieties and carbon, zinc and nitrogen related to the shell parts. As we observed in this image, the morphology of the core parts (Fe and O) is changed after coating with MOFs (C, Zn, and N).^{77–79} For further confirmation of the catalyst preparation, the EDX analysis of bare Fe_3O_4 MNPs and MNP@MOF-PR is performed (Fig. 4). As observed in these figures, after coating the Fe_3O_4 MNPs with MOFs and immobilization of PR HPA, some new peaks corresponding to the MOF structures (C, Zn, and N) and PR HPA (Na, W, P) are observed in the EDX pattern

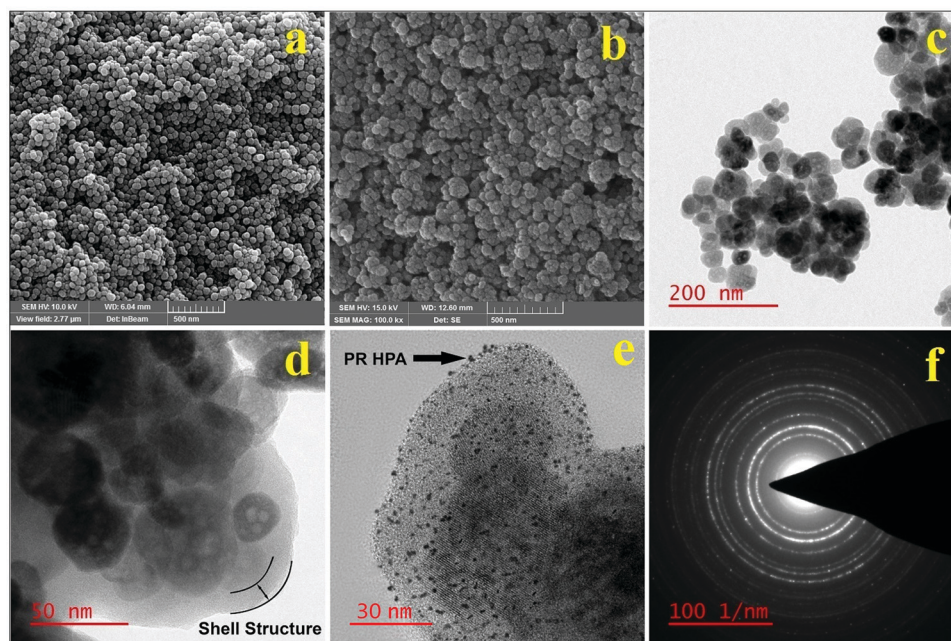


Fig. 2 SEM images of (a) Fe_3O_4 MNPs and (b) MNP@MOF, TEM images of (c) Fe_3O_4 MNPs and (d) MNP@MOF, HRTEM image of (e) MNP@MOF-PR and SAED pattern of (f) MNP@MOF.

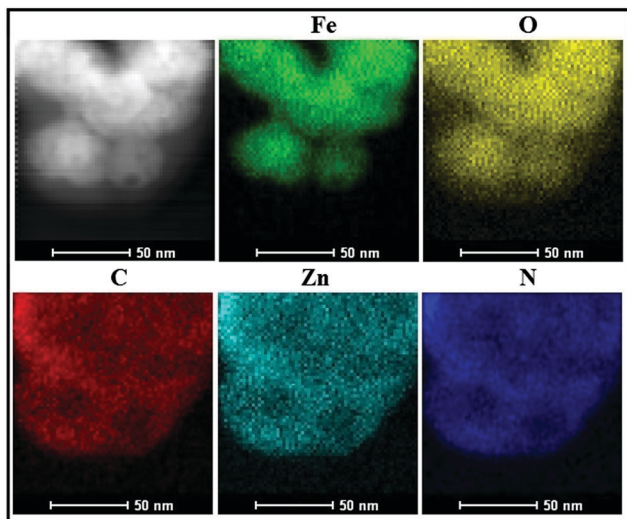


Fig. 3 HRTEM mapping of core-shell MNP@MOF.

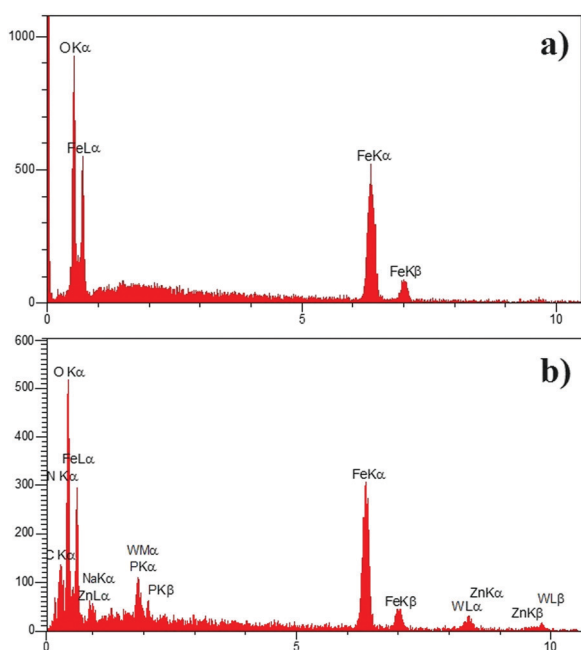


Fig. 4 EDX patterns of (a) Fe_3O_4 MNPs and (b) the final catalyst (MNP@MOF-PR).

of Fe_3O_4 MNPs (Fig. 4a) that confirmed the proper synthesis of shell structures and excellent ionic linkage of PR HPA on the surface of the MOF shells.^{80,81}

Fig. 5 exhibits the XRD patterns for the bare Fe_3O_4 MNPs, pure MOF and core-shell MNP@MOF nanomaterials. The XRD pattern of Fe_3O_4 MNPs (Fig. 5a) shows the crystalline phase characteristics with assignments such as (220), (311), (400), (422), (511) and (440) at $2\theta = 30.1, 35.6, 43.3, 53.3, 57.11$ and 62.10 (JCPDS card no. 19-0629).⁸² The next XRD pattern corresponding to the pure MOF materials with two sharp peaks at around $2\theta = 6.8$ and 9.6 with the lattice planes of (200) and (220) confirms the successful synthesis of MOFs (Fig. 5b).⁶⁵ Finally, it

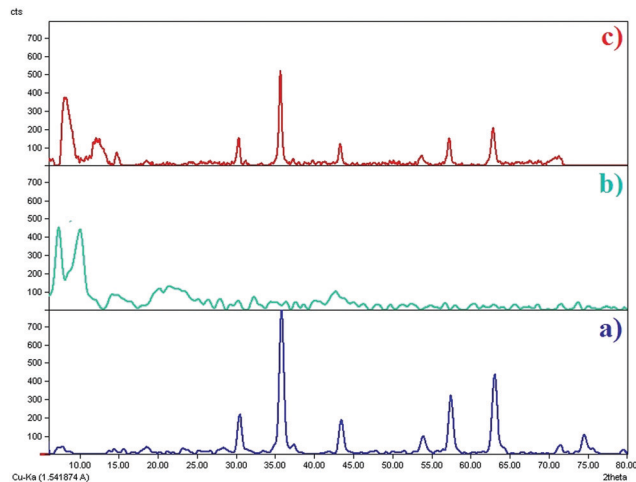


Fig. 5 XRD patterns of (a) Fe_3O_4 MNPs, (b) MOF, and (c) MNP@MOF.

is of prime importance to note that there are XRD peaks of either Fe_3O_4 MNPs or MOFs in the final XRD pattern of the core-shell MNP@MOF materials, which confirm the proper preparation of MNP@MOF nanomaterials (Fig. 5c); however, some moderate shifts are observed in the MOF peaks which probably are attributed to the physical interactions between Fe_3O_4 MNPs and MOF shell structures.

TGA analysis was performed to study the thermal stability of Fe_3O_4 MNPs, core-shell MNP@MOF and PR HPA-immobilized core-shell MNP@MOF (MNP@MOF-PR) under a N_2 flow and running from room temperature to 600°C (Fig. 6 and Fig. S6–S8, ESI[†]). The first graph (Fig. 6a) related to Fe_3O_4 MNPs exhibits 2.27% weight loss at more than 100°C , which can be attributed to decomposition of hydroxyl functional groups on the surface of MNPs. The second graph (Fig. 6b) corresponding to the core-shell MNP@MOFs exhibits two step weight losses, in which the first step that starts at about 100°C is assigned to removal of the remaining trapped solvents and the second weight loss that begins at about 250°C and stretches to 500°C is attributed to decomposition of MOF core structures. The total amount of

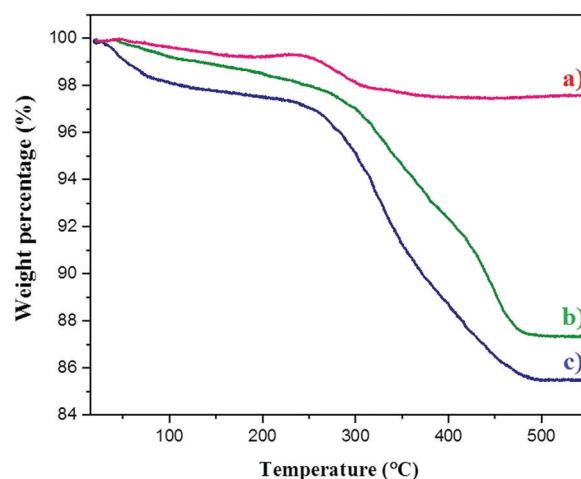


Fig. 6 TGA graph of (a) Fe_3O_4 MNPs, (b) MNP@MOF, and (c) MNP@MOF-PR.

weight loss in this graph is 12.61% and these observations showed that approximately 10% of the catalyst weight is MOF core structures. Eventually, the final TGA graph of PR HPA decorated MNP@MOF (Fig. 6c) is similar to the previous graph and shows about 14.38% weight loss, which confirms that approximately 2.0% of PR HPA was immobilized on the surface of MNP@MOF.⁶⁴ These results confirm the successful synthesis of the catalyst and they are in agreement with the TEM and XRD results.

The VSM technique was the next method for the evaluation of the magnetic properties of the synthesized materials. Thereby, this analysis was also employed for the bare Fe₃O₄ MNPs and the final catalyst including PR HPA decorated MNP@MOF. The Fe₃O₄ MNPs exhibited superparamagnetic properties with a high saturation magnetization at about 86 emu g⁻¹. Interestingly, it was decreased to about 60 emu g⁻¹ after coating the MNPs with MOF core structures and immobilization of PR HPA.^{73,83} These outcomes confirm the successful synthesis of the catalyst and they are in agreement with TEM, XRD and TGA results (Fig. 7).

ICP analysis was examined for the evaluation of both the MOF and the PR HPA catalyst. On this basis, at first, the amount of zinc obtained in the MNP@MOF sample was 5.261 wt%, which firstly confirms again the presence of Zn in the MOF core structures and second, it is in accordance with HRTEM mapping, EDX analysis and the TGA results. Next, the amount of W in the fresh and reused catalysts (after five runs) was also studied with this technique. It was 1.517 and 1.488 wt% for the fresh and reused catalysts, respectively. These outcomes are in accordance with the TGA results, considering the total molecular weight of PR HPA. Besides, the insignificant difference of the amount of W between the fresh and reused catalysts confirms the stable structure of the catalyst and reveals that approximately no leaching of tungsten occurred during the CO₂ fixation reaction.

The pore volume and BET surface area were analyzed using N₂ adsorption/desorption under nitrogen gas (Fig. S9 and S10, ESI†). Both the specific surface area and the pore volume

showed a large decrease after immobilization of the PR HPA into the MNP@MOF structures. The surface area decreased from 301.2 m² g⁻¹ to 121.0 m² g⁻¹ and the average pore volume decreased from 0.483 cm³ g⁻¹ to 0.261 cm³ g⁻¹, respectively. These observations confirmed the successful immobilization of PR HPA on the surface of the MNP@MOF structures.⁶⁴

After complete characterization of the catalyst, its application was examined for the synthesis of cyclic carbonates by the chemical fixation of carbon dioxide. In this regard, the reaction of styrene oxide and carbon dioxide was selected as the model reaction. First, the CO₂ was reacted with styrene oxide at a pressure of 0.5 MPa without the catalyst and no product was observed after 6 h of the reaction (Table 1, entry 1). Second, the model reaction was carried out in the presence of 0.8 mol% of the MNP@MOF-PR catalyst at different temperatures (25, 50, 80 and 100 °C) (Table 1, entries 1–5). The highest amount of 4-phenyl-1,3-dioxolan-2-one (98%) was obtained at 80 °C (Table 1, entry 4) and the upper temperature (100 °C) did not have a significant effect on the reaction yield (Table 1, entry 5). Subsequently, different amounts of the catalyst (0.4, 0.2 and 0.08 mol%) were used in the model reaction at 80 °C (Table 1, entries 6–8). The yields of the reaction were decreased with these amounts and it can be concluded that the best amount is 0.8 mol% that was used in the first experiment. Then, the lower CO₂ pressures were also investigated on the synthesis of 4-phenyl-1,3-dioxolan-2-one (Table 1, entries 9 and 10). With a decrease of the CO₂ pressure to 0.3 and 0.1 MPa, the yields of the reaction were decreased dramatically. To improve the reaction conditions and increase the yields of the reaction, the co-catalyst of tetrabutylammonium bromide (TBAB) was exploited in the model reaction (entries 11–14). Interestingly, 100% of the product yield was isolated in the presence of 10 mol% of TBAB and 0.5 MPa of CO₂ pressure (Table 1, entry 11). Afterwards, only two percent of the yield of the reaction was decreased with half the amount of TBAB (5.0 mol%, Table 1, entry 12). It is worth noting that, even with a decrease of the CO₂ pressure to 0.3 MPa and of the catalyst amount to 0.4 mol%, the yield of the reaction was excellent (96%) and this condition was chosen as the

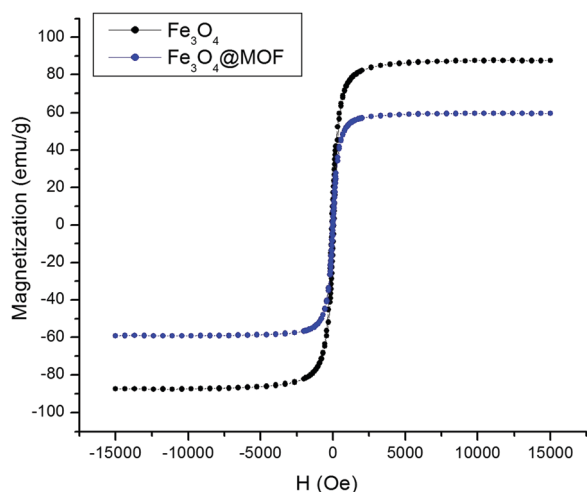


Fig. 7 VSM plot of (a) Fe₃O₄ MNPs and (b) MNP@MOF-PR.

Table 1 Screening of the reaction conditions for the synthesis of **3a**^a

Entry	Temperature (°C)	Catalyst (mg, mol%)	Co-catalyst ^b (mol%)	Pressure (bar)	Time (h)	Yield ^c (%)
1	25	—	—	5.0	6.0	—
2	25	(0.01, 0.8)	—	5.0	2.0	66
3	50	(0.01, 0.8)	—	5.0	2.0	87
4	80	(0.01, 0.8)	—	5.0	2.0	98
5	100	(0.01, 0.8)	—	5.0	2.0	98
6	80	(0.005, 0.4)	—	5.0	2.0	92
7	80	(0.0025, 0.2)	—	5.0	2.0	76
8	80	(0.001, 0.08)	—	5.0	2.0	52
9	80	(0.01, 0.8)	—	3.0	2.0	70
10	80	(0.01, 0.8)	—	1.0	4.0	68
11	80	(0.01, 0.8)	10	5.0	2.0	100
12	80	(0.01, 0.8)	5.0	5.0	2.0	98
13	80	(0.005, 0.4)	5.0	3.0	2.0	96
14	80	(0.001, 0.08)	5.0	5.0	2.0	82

^a Styrene oxide (10 mmol). ^b Tetrabutylammonium bromide. ^c Based on the isolated yields.

final reaction condition (Table 1, entry 13). However, with a decrease of the catalyst amount to 0.08 mol%, the yield of the reaction was not satisfactory (Table 1, entry 14). Therefore, the best reaction condition was the use of 0.4 mol% of the catalyst, at 80 °C and 0.3 MPa of CO₂ pressure and eventually 5.0 mol% of TBAB (Table 1, entry 13).

Due to the significant effect of the co-catalyst on the cycloaddition reaction of epoxides with CO₂, the performance of other co-catalysts such as tetrabutylammonium iodide (TBAI), tetrabutylammonium chloride (TBAC) and trimethylamine (TEA) was compared with that of TBAB in the model reaction at 80 °C and 3.0 bar pressure (Table 2). In the absence of the co-catalyst, only 62% of the styrene carbonate was formed under the reaction conditions. Hence, styrene carbonate **3a** was obtained with 90, 96, 76, and 59% yields, in the presence of TBAI, TBAB, TBAC and TEA, respectively. TBAB showed a superior activity compared with other co-catalysts under similar conditions (Table 2, entry 3).

Encouraged by the excellent activity of our catalyst (MNP@MOF-PR) for the chemical fixation of carbon dioxide in the lower CO₂ pressure (0.3 MPa) and a higher yield of styrene carbonate (96%), in the next step, the efficiency of the catalyst was investigated with other epoxides (Table 3). The catalyst was able to prepare the various epoxides with good to excellent yields (87–98%) and in the presence of 5.0 mol% of TBAB and finally without using any solvent.

Based on our previous studies on the fixation of CO₂,^{11,84} a suggested mechanism for the synthesis of cyclic carbonates in the presence of the catalyst (MNP@MOF-PR) is presented (Scheme 3). As mentioned earlier, the PR HPA catalyst can act as both Brønsted^{85,86} and Lewis acid catalysts^{87,88} due to either proton sites or tungsten elements on its structure (Scheme 3, routes 1 and 2). Hence, as depicted in route 1, owing to the W sites on the catalyst, they can operate as the Lewis acid catalyst and can coordinate to the epoxide and consequently, the activated epoxide is able to react with Br and then CO₂, and finally, cyclic carbonate is formed accordingly. The second path is similar to the previous one, with the difference that the proton sites of the catalyst (Brønsted acid) can activate the reagents and produce the final products (route 2).

In addition, a plausible mechanism of the cycloaddition reaction of epoxy styrene and CO₂ catalyzed by MNP@MOF-PR in the absence of TBAB is shown in Scheme 4. First, the epoxy ring was activated by both the Brønsted and Lewis acid sites of

Table 2 Screening of the effect of other co-catalysts on the synthesis of **3a**

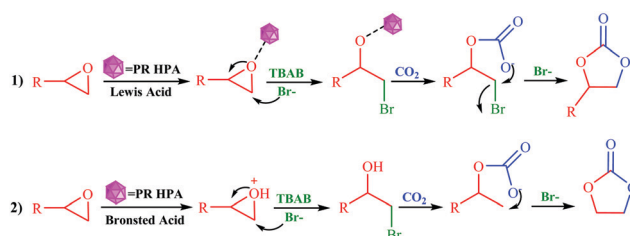
Entry	Temperature (°C)	Catalyst (mg, mol%)	Co-catalyst (mol%)	Pressure (bar)	Time (h)	Yield ^a (%)
1		(0.005, 0.4)	—	3.0	2	62
2	80	(0.005, 0.4)	TBAI	3.0	2	90
3	80	(0.005, 0.4)	TBAB	3.0	2	96
4	80	(0.005, 0.4)	TBAC	3.0	2	76
5	80	(0.005, 0.4)	TEA	3.0	2	59

^a Based on the isolated yields.

Table 3 Synthesis of cyclic carbonates in the presence of the catalyst^a

Entry	Epoxide	Product ^b	Time (min)	Yield ^c (%)
1			120	96
2			150	97
3			150	98
4			90	96
5			120	97
6			270	89
7			120	91
8			150	90
9			240	87

^a Epoxides (10 mmol), TBAB (5.0 mol%), catalyst (0.005 mg, 0.4 mol%) at 0.3 MPa and 80 °C. ^b All the products were characterized by HNMR and CNMR (see the ESI for details). ^c Isolated yields.



Scheme 3 The proposed mechanism for the synthesis of cyclic carbonate in the presence of MNP@MOF-PR as both Lewis (route 1) and Brønsted (route 2) acid catalysts with TBAB.

the nanocatalyst, thereby leading to the formation of intermediate (I). In the following step, the nucleophilic attack of

anion sites ($\text{H}_{13}[\text{NaP}_5\text{W}_{30}\text{O}_{110}]^-$) of the nanocatalyst on the less sterically hindered carbon atom of the epoxide (intermediate (I)) caused the ring-opening to form intermediate (II). Then, acyclic carbonate (intermediate (III)) was formed by the nucleophilic attack of the oxygen atom of intermediate (II) to CO_2 . Finally, the cyclic carbonate (IV) is achieved by intramolecular cyclization without the co-catalyst.

The prepared nanomagnetic catalyst can be used in many repeated model reactions. Thus, for the confirmation of this claim, the stability and efficiency of the heterogeneous catalyst were studied in the five repeated model reactions. On this basis, after finalization of the CO_2 fixation reaction, ethyl acetate was added to the reaction mixture and MNP@MOF-PR was separated from the reaction mixture by an external magnet and then it was rinsed many times with ethyl acetate and H_2O and dried in a vacuum oven at 75°C for 6 h for further re-use. As it is evident from Fig. 8, the catalyst is able to synthesize the carbonates after reuse five times without any significant decrease in catalytic activity. Also, as mentioned before, the amount of W was also studied by ICP analysis after five times reusing the catalyst, and the ICP results did not show any significant difference between the fresh and reused catalysts. Furthermore, any structural changes of the catalyst were studied by FT-IR, TGA and SEM techniques. It is clearly evident from the FT-IR spectrum of the 5th reused catalyst that the PR HPA ions were strongly bound to the surface of MNP@MOF through the ionic linkage, and no important changes in the intensities, frequencies, and shapes of the absorption bands were observed (Fig. S11, ESI[†]). Interestingly, comparing the TGA plots of the fresh (Fig. S8, ESI[†]) and 5th reused catalysts (Fig. S12, ESI[†]) showed that no significant changes in weight loss were observed and important weight losses were similar in the two plots. In addition, the size and morphology of the reused catalyst were investigated by the SEM technique (Fig. S13, ESI[†]). This image was approximately similar to the SEM image of the fresh catalyst (Fig. 2b) and there are no significant differences in the size and morphology. These outcomes confirm that the PR HPA strongly connected to the amine groups of the MOF shell structures by ionic bonding and during the reaction, they do not separate from the MOF structures and the structure of the catalyst remained stable and

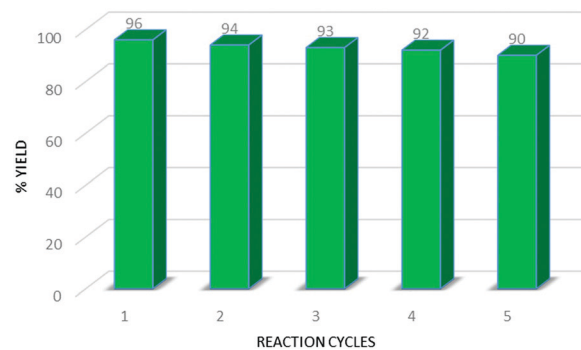


Fig. 8 Reusability of the catalyst for the model reaction.

no leaching of PR HPA as the catalyst occurred during the reaction.

The hot filtration test was another analysis to confirm the heterogeneous nature of MNP@MOF-PR in the chemical fixation of carbon dioxide. Hence, the model reaction was studied again under the optimized reaction conditions. After 60 min of the reaction (50% conversion), the reactor was allowed to cool down to room temperature and CO_2 was vented gradually. After this, ethyl acetate was added to the reaction mixture and the MNP@MOF-PR was separated from the reaction mixture by an external magnet. Next, the rest of the reaction was carried out in the absence of the catalyst for a further 60 min. Observations showed that the reaction did not intend to move forward and confirmed that no leaching of PR HPA occurred during the reaction. These results are in accordance with the reusability test of the catalyst and ICP results as well.

The efficiency and capability of the PR HPA-immobilized MNP@MOF catalyst were compared with other reported catalysts for the cyclic synthesis of styrene carbonate *via* the chemical fixation of carbon dioxide (Table 4). The results show that the catalyst can catalyze the synthesis of styrene carbonate in a shorter reaction time (2.0 h) compared with other catalysts (3.0–48 h) and also a higher amount of yield (Table 4, entries 1–4, 6 and 8). However, the CO_2 pressure (0.3 MPa) was lower compared to some methods (Table 3, entries 1–4), but it was higher compared to others (Table 4, entries 5–8).

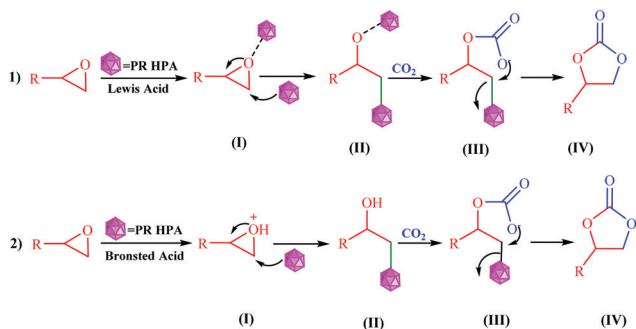
Experimental

General

All the materials and reagents were purchased from Sigma-Aldrich and Merck and used without any further purification.

Preparation of the catalyst (MNP@MOF-PR)

For preparation of the catalyst, first, Fe_3O_4 MNPs were synthesized by using FeCl_3 and the hydrothermal process,⁶⁷ and then these synthesized MNPs with size below 50 nm were coated with amino-functionalized MOF (IRMOF-3) by the solvothermal reaction of zinc nitrate and 2-aminoterephthalic acid (ATA).⁶⁵ For this purpose, 1.0 g of polyvinyl pyrrolidone (PVP) was dissolved in a mixture of 20 mL of ethanol and 30 mL of DMF. On the other hand, 40 mg of Fe_3O_4 MNPs were dispersed in 2.0 mL of ethanol ultrasonically for 20 min and then this



Scheme 4 The proposed mechanism for the synthesis of cyclic carbonate in the presence of MNP@MOF-PR as both Lewis (route 1) and Brønsted (route 2) acid catalysts and without TBAB.

Table 4 Comparison of the MNP@MOF-PR catalyst with other catalysts for the synthesis of styrene carbonate **3a**

Entry	Catalyst	Condition	Co-catalyst	Temperature (°C)	Pressure (MPa)	Time (h)	Yield (%)	Ref.
1	Nb ₂ O ₅	DMF	—	135	5.0	15	80	89
2	La-Zr oxide	DMF	—	130	2.5	3.0	90	90
3	Zn-Mg-Al	TEA	—	140	2.5	3.0	89	91
4	CuCo ₂ O ₄	Sol. free	TBAI ^a	80	2.0	3.0	88	92
5	Zn MOF	Sol. free	TBAB	60	0.1	8.0	99	93
6	COF-JLU7	Sol. free	TBAB	40	0.1	48	88	94
7	ZnO@NPC-Ox	CH ₃ CN	TBAB	60	0.1	48	98	95
8	Cationic MOF	Sol. free	TBAB	80	0.1	4.0	90	96
9	CuAl ₂ O ₄	Sol. free	TBAB	85	0.3	10	98	11
10	MNP@MOF-PR ^b	Sol. free	TBAB	80	0.3	2.0	96	—

^a Tetrabutylammonium iodide. ^b Present study.

mixture was added drop by drop to the previously prepared solution under stirring. Subsequently, 111.55 mg of zinc nitrate (0.375 mmol) and 27.15 mg of 2-aminoterephthalic acid (0.15 mmol) were dissolved in 10 mL of DMF and added to the previous solution. Afterwards, the mixture was dispersed ultrasonically for 15 min and then it was transferred to a 100 mL Teflon-lined stainless steel autoclave and heated at 100 °C for 5 h. After this, the synthesized core-shell MNP@MOF materials were collected by an external magnet and in order to remove the unreacted ATA and PVP, the synthesized solid product was re-dispersed in 30 mL of DMF and heated in an autoclave at 100 °C for 12 h. Finally, the pure core-shell MNPs were separated from the solution by an external magnet and then it was rinsed with DMF and ethanol and dried in a vacuum oven at 50 °C for 12 h. Eventually, the PR HPA was immobilized to the amine groups on the surface of the core-shell MNP@MOFs by the ionic bonds with the following procedure. Hence, 50 mg of PR HPA was dissolved in 5.0 mL of methanol and then it was added dropwise to a suspension of 100 mg of the prepared core-shell MNP@MOF material in 5.0 mL of methanol. This mixture was stirred for 12 h and then the solid PR HPA-immobilized MNP@MOF was separated from the solution by an external magnet and dried in a vacuum oven at 50 °C for 12 h to obtain the final catalyst (MNP@MOF@PR).⁷⁰

General procedure for the chemical fixation of CO₂ with different epoxides

First, a stainless steel high pressure batch reactor was prepared for the reaction. Then, 10 mmol of epoxide was loaded onto the reactor and subsequently, 5.0 mmol of TBAB (co-catalyst) and an appropriate amount of the catalyst were added to the reactor and the mixture was heated at 80 °C. The reaction was carried out for the specified durations as shown in Table 2, while the reactor pressure was kept constant with CO₂ at a reaction pressure in the range of 0.1–0.5 MPa. Eventually, after completion of the reaction, the reactor was allowed to cool down to room temperature and CO₂ was vented gradually. After this, ethyl acetate was added to the reaction mixture and the MNP@MOF-PR was separated from the reaction mixture by an external magnet and then it was rinsed many times with ethyl acetate and H₂O and dried in a vacuum oven at 75 °C for 6 h and for further re-use. Some water was added to the remaining reaction

mixture to remove the co-catalyst and unreacted reagents and finally, the organic layers were dried with sodium sulfate. The obtained carbonates were purified by column chromatography using ethyl acetate–hexane. The structures of all the products were characterized by using ¹H-NMR and ¹³C-NMR (see ESI†).

Conclusion

In summary, a new magnetic MOF platform was introduced for ionic immobilization of PR HPA. On this basis, the core-shell magnetic MOFs were synthesized and then the PR HPA was immobilized on the surface of the MOF shell structures by the ionic reaction between the proton sites of PR HPA and the amine groups of the MOF. The electronic microscopic observations, IR, TGA and ICP analysis confirmed the core-shell structures and the proper decoration of PR HPA on the MOF materials. This new supporting magnetic platform can be used in the post-synthesis modification in the design and preparation of various catalysts by chemical and physical immobilization of different organic ligands and complexes and also homogeneous catalysts. Moreover, this catalyst can be operated as both Lewis and Brønsted acid catalysts for the synthesis of cyclic carbonates *via* the chemical fixation of carbon dioxide. Eventually, due to the excellent paramagnetic properties, it can be reused in several repeated reactions without a significant decrease in catalytic activity and leaching behavior.

Conflicts of interest

There are no conflicts to declare.

Acknowledgements

The authors gratefully acknowledge partial support of this study by the Mashhad University of Medical Sciences and the Shiraz University of Technology.

References

- 1 G. A. Meehl and W. M. Washington, *Nature*, 1996, **382**, 56–60.
- 2 M. He, Y. Sun and B. Han, *Angew. Chem., Int. Ed.*, 2013, **52**, 9620–9633.

- 3 T. Sakakura, J.-C. Choi and H. Yasuda, *Chem. Rev.*, 2007, **107**, 2365–2387.
- 4 Z.-Z. Yang, Y. Zhao, G. Ji, H. Zhang, B. Yu, X. Gao and Z. Liu, *Green Chem.*, 2014, **16**, 3724–3728.
- 5 B. Schaffner, F. Schaffner, S. P. Verevkin and A. Borner, *Chem. Rev.*, 2010, **110**, 4554–4581.
- 6 J. P. Vivek, N. Berry, G. Papageorgiou, R. J. Nichols and L. J. Hardwick, *J. Am. Chem. Soc.*, 2016, **138**, 3745–3751.
- 7 L. C. Yang, Z. Q. Rong, Y. N. Wang, Z. Y. Tan, M. Wang and Y. Zhao, *Angew. Chem., Int. Ed.*, 2017, **56**, 2927–2931.
- 8 H. Liu, Z. Huang, Z. Han, K. Ding, H. Liu, C. Xia and J. Chen, *Green Chem.*, 2015, **17**, 4281–4290.
- 9 H. Ji, K. Naveen, W. Lee, T. S. Kim, D. Kim and D.-H. Cho, *ACS Appl. Mater. Interfaces*, 2020, **12**, 24868–24876.
- 10 K. Naveen, H. Ji, T. S. Kim, D. Kim and D.-H. Cho, *Appl. Catal., B*, 2021, **280**, 119395.
- 11 R. Khalifeh, M. Karimi, M. Rajabzadeh, A. Hafizi and F. S. Nogorani, *J. CO₂ Util.*, 2020, **41**, 101233.
- 12 D.-H. Lan, H.-T. Wang, L. Chen, C.-T. Au and S.-F. J. C. Yin, *Carbon*, 2016, **100**, 81–89.
- 13 D.-H. Lan, Y.-X. Gong, N.-Y. Tan, S.-S. Wu, J. Shen, K.-C. Yao, B. Yi, C.-T. Au and S.-F. J. C. Yin, *Carbon*, 2018, **127**, 245–254.
- 14 L. Gloag, M. Mehdipour, D. Chen, R. D. Tilley and J. J. Gooding, *Adv. Mater.*, 2019, **31**, 1904385.
- 15 A. Goldman, *Modern ferrite technology*, Springer Science & Business Media, 2006.
- 16 E. Teymouri, A. Davoodnia, A. Khojastehnezhad and N. Hosseininasab, *Iran. Chem. Commun.*, 2019, **7**, 271–282.
- 17 F. Moeinpour and A. Khojastehnezhad, *Arabian J. Chem.*, 2017, **10**, S3468–S3474.
- 18 A. Khojastehnezhad, B. Maleki, B. Karrabi and E. R. Seresht, *Org. Prep. Proced. Int.*, 2017, **49**, 338–345.
- 19 N. Hosseininasab, A. Davoodnia, F. Rostami-Charati and A. Khojastehnezhad, *Russ. J. Gen. Chem.*, 2017, **87**, 2436–2443.
- 20 A. Javid, A. Khojastehnezhad, H. Eshghi, F. Moeinpour, F. F. Bamoharram and J. Ebrahimi, *Org. Prep. Proced. Int.*, 2016, **48**, 377–384.
- 21 B. Maleki, S. Barat Nam Chalaki, S. Sedigh Ashrafi, E. Rezaee Seresht, F. Moeinpour, A. Khojastehnezhad and R. Tayebee, *Appl. Organomet. Chem.*, 2015, **29**, 290–295.
- 22 B. Maleki, H. Eshghi, M. Barghamadi, N. Nasiri, A. Khojastehnezhad, S. S. Ashrafi and O. Pourshiani, *Res. Chem. Intermed.*, 2016, **42**, 3071–3093.
- 23 S. Sonei, F. Taghavi, A. Khojastehnezhad and M. Gholizadeh, *ChemistrySelect*, 2021, **6**, 359–368.
- 24 J. Jin, T. Iyoda, C. Cao, Y. Song, L. Jiang, T. J. Li and D. B. Zhu, *Angew. Chem., Int. Ed.*, 2001, **113**, 2193–2196.
- 25 J.-E. Bae, M.-I. Huh, B.-K. Ryu, J.-Y. Do, S.-U. Jin, M.-J. Moon, J.-C. Jung, Y. Chang, E. Kim and S.-G. Chi, *Biomaterials*, 2011, **32**, 9401–9414.
- 26 T. J. Yoon, H. Lee, H. Shao and R. Weissleder, *Angew. Chem., Int. Ed.*, 2011, **123**, 4759–4762.
- 27 H. Zhang, D. Pan, K. Zou, J. He and X. Duan, *J. Mater. Chem.*, 2009, **19**, 3069–3077.
- 28 H. Eshghi, A. Javid, A. Khojastehnezhad, F. Moeinpour, F. F. Bamoharram, M. Bakavoli and M. Mirzaei, *Chin. J. Catal.*, 2015, **36**, 299–307.
- 29 H. Eshghi, A. Khojastehnezhad, F. Moeinpour, M. Bakavoli, S. M. Seyedi and M. Abbasi, *RSC Adv.*, 2014, **4**, 39782–39789.
- 30 B. Maleki, M. Baghayeri, S. A. J. Abadi, R. Tayebee and A. Khojastehnezhad, *RSC Adv.*, 2016, **6**, 96644–96661.
- 31 K. M. Ho and P. Li, *Langmuir*, 2008, **24**, 1801–1807.
- 32 A. Khojastehnezhad, F. Moeinpour and A. Javid, *Polycyclic Aromat. Compd.*, 2019, **39**, 404–412.
- 33 M. Rahimizadeh, S. M. Seyedi, M. Abbasi, H. Eshghi, A. Khojastehnezhad, F. Moeinpour and M. Bakavoli, *J. Iran. Chem. Soc.*, 2015, **12**, 839–844.
- 34 F. Ke, L.-G. Qiu, Y.-P. Yuan, X. Jiang and J.-F. Zhu, *J. Mater. Chem.*, 2012, **22**, 9497–9500.
- 35 Y. Guo, L. Zhang, X. Liu, B. Li, D. Tang, W. Liu and W. Qin, *J. Mater. Chem.*, 2016, **4**, 4044–4055.
- 36 C. Hou, D. Zhao, W. Chen, H. Li, S. Zhang and C. Liang, *Nanomaterials*, 2020, **10**, 426.
- 37 S. Rayati, F. Nejabat and F. Panjiali, *Catal. Commun.*, 2019, **122**, 52–57.
- 38 A. Khorshidi and S. Shariati, *RSC Adv.*, 2014, **4**, 41469–41475.
- 39 C. Gao, J. Bai, Y. He, Q. Zheng, W. Ma, Z. Lei, M. Zhang, J. Wu, F. Fu and Z. Lin, *ACS Appl. Mater. Interfaces*, 2019, **11**, 13735–13741.
- 40 S. Swami, A. Agarwala and R. Shrivastava, *New J. Chem.*, 2016, **40**, 9788–9794.
- 41 B. Zuo, W. Li, X. Wu, S. Wang, Q. Deng and M. Huang, *Chem. – Asian J.*, 2020, **15**, 1248–1265.
- 42 A. Farrokhi, K. Ghodrati and I. Yavari, *Catal. Commun.*, 2015, **63**, 41–46.
- 43 N. Fattahi, A. Ramazani and V. Kinzhybalov, *Silicon*, 2019, **11**, 1745–1754.
- 44 H. Naeimi and S. Mohamadabadi, *Dalton Trans.*, 2014, **43**, 12967–12973.
- 45 C. S. Gill, B. A. Price and C. W. Jones, *J. Catal.*, 2007, **251**, 145–152.
- 46 B. Maleki, H. Eshghi, A. Khojastehnezhad, R. Tayebee, S. S. Ashrafi, G. E. Kahoo and F. Moeinpour, *RSC Adv.*, 2015, **5**, 64850–64857.
- 47 A. Khojastehnezhad, M. Rahimizadeh, H. Eshghi, F. Moeinpour and M. Bakavoli, *Chin. J. Catal.*, 2014, **35**, 376–382.
- 48 C. Zhang, H. Chen, M. Ma and Z. Yang, *J. Mol. Catal.*, 2015, **402**, 10–16.
- 49 M. A. Zolfigol and M. Yarie, *Appl. Organomet. Chem.*, 2017, **31**, e3598.
- 50 H. Woo and K. H. Park, *Catal. Commun.*, 2014, **46**, 133–137.
- 51 Q. An, M. Yu, Y. Zhang, W. Ma, J. Guo and C. Wang, *J. Phys. Chem. C*, 2012, **116**, 22432–22440.
- 52 H.-C. Zhou, J. R. Long and O. M. Yaghi, *Chem. Rev.*, 2012, **112**, 673–674.
- 53 O. K. Farha and J. T. Hupp, *Acc. Chem. Res.*, 2010, **43**, 1166–1175.
- 54 N. L. Rosi, J. Eckert, M. Eddaoudi, D. T. Vodak, J. Kim, M. O’Keeffe and O. M. Yaghi, *Science*, 2003, **300**, 1127–1129.
- 55 X. Ma, Y. Chai, P. Li and B. Wang, *Acc. Chem. Res.*, 2019, **52**, 1461–1470.

- 56 Z. Luo, S. Fan, C. Gu, W. Liu, J. Chen, B. Li and J. Liu, *Curr. Med. Chem.*, 2019, **26**, 3341–3369.
- 57 X. Zhu, H. Zheng, X. Wei, Z. Lin, L. Guo, B. Qiu and G. Chen, *Chem. Commun.*, 2013, **49**, 1276–1278.
- 58 F. Gao, X. Tu, X. Ma, Y. Xie, J. Zou, X. Huang, F. Qu, Y. Yu and L. Lu, *Talanta*, 2020, **215**, 120891.
- 59 A. Herbst, A. Khutia and C. Janiak, *Inorg. Chem.*, 2014, **53**, 7319–7333.
- 60 W. Li, X. Wu, S. Li, W. Tang and Y. Chen, *Appl. Surf. Sci.*, 2018, **436**, 252–262.
- 61 S. Yang, Z. H. Zhang, Q. Chen, M. Y. He and L. Wang, *Appl. Organomet. Chem.*, 2018, **32**, e4132.
- 62 F. Ke, L.-G. Qiu and J. Zhu, *Nanoscale*, 2014, **6**, 1596–1601.
- 63 S. Chang, C. Liu, Y. Sun, Z. Yan, X. Zhang, X. Hu and H. Zhang, *ACS Appl. Mater. Interfaces*, 2020, **3**, 2302–2309.
- 64 M. M. Mostafavi and F. Movahedi, *Eur. J. Inorg. Chem.*, 2019, 787–793.
- 65 M. Zhao, K. Deng, L. He, Y. Liu, G. Li, H. Zhao and Z. Tang, *J. Am. Chem. Soc.*, 2014, **136**, 1738–1741.
- 66 G. Gao, J.-Q. Di, H.-Y. Zhang, L.-P. Mo and Z.-H. Zhang, *J. Catal.*, 2020, **387**, 39–46.
- 67 S. Xuan, F. Wang, Y.-X. J. Wang, C. Y. Jimmy and K. C.-F. Leung, *J. Mater. Chem.*, 2010, **20**, 5086–5094.
- 68 R. Tayebee, M. Amini, M. Akbari and A. Aliakbari, *Dalton Trans.*, 2015, **44**, 9596–9609.
- 69 A. Hashemzadeh, M. M. Amini, R. Tayebee, A. Sadeghian, L. J. Durndell, M. A. Isaacs, A. Osatiashtiani, C. M. Parlett and A. F. Lee, *Mol. Catal.*, 2017, **440**, 96–106.
- 70 H. Eshghi, A. Khojastehnezhad, F. Moeinpour, S. Rezaeian, M. Bakavoli, M. Teymouri, A. Rostami and K. Haghbeen, *Tetrahedron*, 2015, **71**, 436–444.
- 71 L. Lili, Z. Xin, G. Jinsen and X. Chunming, *Green Chem.*, 2012, **14**, 1710–1720.
- 72 F. Nouri, S. Rostamizadeh and M. Azad, *Mol. Catal.*, 2017, **443**, 286–293.
- 73 L. Zhao, Y. Chi, Q. Yuan, N. Li, W. Yan and X. Li, *J. Colloid Interface Sci.*, 2013, **390**, 70–77.
- 74 J. Dou and H. C. Zeng, *J. Am. Chem. Soc.*, 2012, **134**, 16235–16246.
- 75 O. Makrygenni, E. Secret, A. Michel, D. Brouri, V. Dupuis, A. Proust, J.-M. Siaugue and R. Villanneau, *J. Colloid Interface Sci.*, 2018, **514**, 49–58.
- 76 Q. Xing, Z. Han and S. Zhao, *Mater. Lett.*, 2017, **188**, 103–106.
- 77 Y. Benseghir, A. Lemarchand, M. Duguet, P. Mialane, M. Gomez-Mingot, C. Roch-Marchal, T. Pino, M.-H. Ha-Thi, M. Haouas and M. Fontecave, *J. Am. Chem. Soc.*, 2020, **142**, 9428–9438.
- 78 S. Venkateswarlu, A. Panda, E. Kim and M. Yoon, *ACS Appl. Nano Mater.*, 2018, **1**, 4198–4210.
- 79 R. Ma, P. Yang, Y. Ma and F. Bian, *ChemCatChem*, 2018, **10**, 1446–1454.
- 80 A. Akbari, M. Chamack and M. Omidkhan, *J. Mater. Sci.*, 2020, **55**, 6513–6524.
- 81 M. Taheri and R. Mohebat, *J. Mater. Sci.: Mater. Electron.*, 2021, 1–12.
- 82 B. Y. Yu and S.-Y. Kwak, *J. Mater. Chem.*, 2010, **20**, 8320–8328.
- 83 S. Chang, C. Liu, Y. Sun, Z. Yan, X. Zhang, X. Hu and H. Zhang, *ACS Appl. Nano Mater.*, 2020, **3**, 2302–2309.
- 84 M. Rajabzadeh, R. Khalifeh, H. Eshghi and A. Hafizi, *J. Ind. Eng. Chem.*, 2020, **89**, 458–469.
- 85 H. Shen, Y. Li, S. Huang, K. Cai, Z. Cheng, J. Lv and X. Ma, *Catal. Today*, 2019, **330**, 117–123.
- 86 J. Pedada, H. B. Friedrich and S. Singh, *J. Am. Chem. Soc.*, 2018, **15**, 1411–1418.
- 87 D. Zhang, W. Zhang, Z. Lin, J. Dong, N. Zhen, Y. Chi and C. Hu, *Inorg. Chem.*, 2020, **59**, 9756–9764.
- 88 C. N. Kato, T. Ogasawara, A. Kondo and D. Kato, *Catal. Commun.*, 2017, **96**, 41–45.
- 89 M. Aresta, A. Dibenedetto, L. Gianfrate and C. Pastore, *J. Mol. Catal.*, 2003, **204**, 245–252.
- 90 P. R. Tambe and G. D. Yadav, *Clean Technol. Environ. Policy*, 2018, **20**, 345–356.
- 91 W.-L. Dai, S.-F. Yin, R. Guo, S.-L. Luo, X. Du and C.-T. Au, *Catal. Lett.*, 2010, **136**, 35–44.
- 92 D. Prasad, K. N. Patil, J. T. Bhanushali, B. M. Nagaraja and A. H. Jadhav, *Catal. Sci. Technol.*, 2019, **9**, 4393–4412.
- 93 Y.-L. Wu, G.-P. Yang, S. Cheng, J. Qian, D. Fan and Y.-Y. Wang, *ACS Appl. Mater. Interfaces*, 2019, **11**, 47437–47445.
- 94 Y. Zhi, P. Shao, X. Feng, H. Xia, Y. Zhang, Z. Shi, Y. Mu and X. Liu, *J. Mater. Chem.*, 2018, **6**, 374–382.
- 95 M. Ding, S. Chen, X. Q. Liu, L. B. Sun, J. Lu and H. L. Jiang, *ChemSusChem*, 2017, **10**, 1898–1903.
- 96 C. Yao, S. Zhou, X. Kang, Y. Zhao, R. Yan, Y. Zhang and L. Wen, *Inorg. Chem.*, 2018, **57**, 11157–11164.